Collective and single particle structure in ^{103}Rh

H. Dejbakhsh, R. P. Schmitt, and G. Mouchaty
Cyclotron Institute, Texas A&M University, College Station, Texas 77843
(Received 22 July 1987)

High-spin states in ^{103}Rh have been studied using the ^{100}Mo(^{7}Li,4nγ) reaction at 45 MeV. The in-beam techniques employed included relative γ-ray excitation functions, γ-γ coincidences, and γ-ray angular distribution measurements. Low-lying collective bands built on the $1g_{9/2}$ and $2p_{1/2}$ quasiproton states show large signature splitting. At higher excitation energies (2.346 and 3.399 MeV), two strong $\Delta I=1$ cascades are also observed with small signature splitting. These latter bands probably arise from three quasiparticle configurations. The one quasiparticle bands are interpreted within the framework of the axially symmetric rotor-plus-particle model with a variable moment of inertia, the generalized particle-asymmetric-rotor model, and the interacting boson-fermion model. High-spin features of ^{103}Rh are compared with the predictions of the cranked shell model. All of the models indicate that ^{103}Rh is a soft nucleus which exhibits shape coexistence.

I. INTRODUCTION

Even-even $A\approx100$ nuclides with $40\leq Z\leq50$ and $N>50$ are of current interest because of the nature of the shape transitions which occur in this region. A sudden shape transition from spherical to stable prolate deformations is observed in even-even Zr and Mo isotopes between 58 and 60 neutrons.[1,2] The subshell closures at $Z=40$ and $N=56$ have been shown to be the cause of this abrupt shape change.[3] Explicit shell model calculations for Zr and Mo isotopes have been carried out by Federman and Pittel[4,5] to explain the onset of deformation at $N=60$. According to their investigations the shape change results from the strong attractive interaction between neutron and proton orbitals with large spatial overlap, such as the spin-orbit partner orbitals (SOP) $\pi g_{9/2}$ and $\nu g_{7/2}$. The n-p interaction is most effective in driving the deformation force when the SOP orbitals are near the Fermi surface.

As the number of protons increases, the shape transition becomes more gradual. However, the nature of the shape transition in the $Z>42$ and $N>56$ region is not well understood. In part, this is reflected in the level structures of the ($Z\geq42, N\geq56$) nuclei such as Ru, Rh, Pd, and Ag isotopes. These nuclei have features which can be reproduced by vastly different models. Extensive calculations have been reported using the symmetric rotor-plus-particle model, the interacting boson model (IBM), the interacting boson fermion model (IBFM) and the generalized particle-asymmetric-rotor model. The symmetric rotor model has been partially successful in describing even-even Pd isotopes and odd-A Ru, Pd, and Ag isotopes as slightly deformed prolate rotors.[6–9] The $^{105-109}$Ag isotopes, on the other hand, have been treated as asymmetric rotors with large γ deformations.[10] The even-even Ru and Pd isotopes have been described as γ unstable with the IBM-2 model[11] while the IBM-1 model predicts some of these same nuclei to be anharmonic vibrators.[12] While evidence for asymmetric deformations in Ru isotopes has been reported in Refs. 13 and 14, the experimental quadrupole moments for ^{103}Rh and ^{104}Pd indicate small prolate deformations.[15–17]

Some of the uncertainties in the shapes of nuclides in the $40<Z<50, N>50$ region are also apparent from energy surface calculations. Over the past 20 years, many of these calculations have been reported using different models. Prolate,[18] oblate,[19] and asymmetric[20] shapes have been predicted for the ground states of these nuclei. The energy surface calculations and the fits obtained with different models strongly suggest that these nuclei are soft in shape. In the $A\approx100$ region ($44\leq Z\leq50$ and $N>54$) different types of deformations (i.e., prolate, oblate, or triaxial) seem to be possible. Moreover, a coexistence of different types of deformation may occur in the same nucleus.

The behavior of nuclei in the $A\approx100$ region at higher excitation energies and higher spins is also of interest. In general, the alignment of a pair of particles along the axis of collective rotation is expected to be superimposed on the low lying collective structure causing the irregularity in the band structure commonly known as backbending. This feature is well documented in the rare-earth region.[21] In this case, the alignment of a pair of $i_{13/2}$ neutrons is observed for $I=10-14$ at a rotational frequency of $\omega\approx0.3$ MeV/$\hbar$. In the $A\approx80$ region (e.g., the Kr isotopes), backbending is observed at lower spin ($I=8$) due to alignment of pair of $g_{9/2}$ protons at a higher frequency of $\omega\approx0.5$ MeV/$\hbar$. Band crossing has been associated with nuclear shape changes in the rare-earth[22,23] and the mass 80 regions[24] because of the disappearance of signature splitting and the increase in $M1$ transitions probabilities after the crossing. So far band crossing in the $A\approx100$ region has received relatively little attention. The alignment of a pair of $h_{11/2}$ neutrons in ^{102}Ru, ^{104,106}Pd, and ^{107}Ag is observed for $I\approx10$ at a crossing frequency of $\omega\approx0.4$ MeV/$\hbar$. Recently, Frauendorf[25] has applied the concept of configuration dependent triaxiality to transitional Ag isotopes (^{105}Ag and

^{107}Ag) where strong changes in γ are induced by $\pi g_{9/2}$ and $\nu h_{11/2}$ quasiparticles. According to Frauendorf,[25] a configuration dependent γ is expected for transitional nuclei where the Fermi surface lies in a different part of the intruder j shell ($\pi g_{9/2}$ and $\nu h_{11/2}$). This feature has been predicted by cranked shell model (CSM) calculations. A recent blocking experiment has been reported which discusses the band crossing in the $A \approx 100$ region.[26]

The validity of the various theoretical predictions mentioned above can be established from systematic investigations of sequences of isotopes and isotones. The odd-proton nucleus, ^{103}Rh, which is the subject of this study, is of particular interest since, with 45 protons, it is situated halfway between the $Z=40$ subshell closure and the $Z=50$ shell closure and with 58 neutrons it lies at the edge of the strongly deformed region. Since the $1g_{9/2}$ proton orbital is filled between $Z=40$ and $Z=50$, the features of the odd-proton nucleus ^{103}Rh are expected to be affected, not only by the number of protons or proton holes in the $\pi g_{9/2}$ orbital, but also by the number of neutrons in the $\nu h_{11/2}$ orbital. Therefore, when studying ^{103}Rh the interplay between collective and single-particle degrees of freedom should be considered.

Low spin states in ^{103}Rh have been studied by the decay of ^{103}Ru and ^{103}Pd, by Coulomb excitation[27,28] and by particle spectroscopy using various reactions.[29] High-spin states were not known when this study started. While this work was in progress, two other in-beam studies of ^{103}Rh were reported: Kajrys *et al.*[30] used the ^{100}Mo(^{6}Li,3nγ) reaction at 25 MeV, and Charvet *et al.*[31] studied the ^{100}Mo(^{7}Li,4nγ) reaction at 28 MeV. In the current work the structure of ^{103}Rh was investigated by means of ^{100}Mo(^{7}Li,4nγ) reaction at 45 MeV. Several well developed bands are observed, the main features of which have been reported earlier.[32,33] The present level scheme contains 15 new high-spin levels and twice as many transitions as have been published so far. The differences between the previous studies and the present work will be discussed below.

The experimental procedure and data analysis are described in Sec. II. Experimental results are presented in Sec. III. Section IV is devoted to the model calculations and their comparison with the experimental results. Conclusions from this study are given in Sec. V.

II. EXPERIMENTAL PROCEDURE

The data were obtained by applying standard in-beam γ-ray spectroscopy to the ^{100}Mo(^{7}Li,4nγ) reaction. An enriched, self-supporting target of ^{100}Mo (≈ 2 mg/cm^2) was bombarded with ^{7}Li beams from the Texas A&M University Cyclotron. Gamma rays were detected using 20% coaxial Ge(Li) counters which had energy resolution in the range of 2.0–2.5 keV full width at half maximum (FWHM) at 1332 keV. The nonlinearity of the system and energy calibrations were determined with ^{152}Eu, ^{133}Ba, and ^{60}Co standard sources, which cover the range between 80 and 1500 keV.

Measurements of the γ-ray yields at two beam energies (45 and 49 MeV ^{7}Li) helped in assigning γ rays to specific Rh isotopes. On the basis of these measurements, the 45 MeV bombarding energy was chosen to optimize the relative yields of γ-ray transitions in ^{103}Rh. Some of the γ-ray transitions observed arose from charged particle emission (p, d, t, and α), due to both massive transfer reactions (break-up fusion) and evaporation from the compound nucleus. The products identified in the γ-ray spectra were as follows: ^{102}Rh from 5n, ^{103}Rh from 4n, $^{101-104}$Ru from p, d, or tχnγ channels, ^{101}Tc from α2nγ, and ^{102}Mo from αpγ or ^{5}Li emission. Our previous massive transfer measurements[26] for the same reaction were of a great help in assigning and identifying the various transitions in the complicated spectrum. Figure 1 shows the singles spectrum of the ^{100}Mo(^{7}Li,4nγ) reaction at 45 MeV. Most of the lines which have not been labeled belong to ^{102}Rh. The complexity of the spectrum and the appreciable yield of the other exit channels can be seen in greater detail in Fig. 2. Here fits are shown for two different regions of the singles spectrum (beginning at 300 and 660 keV, respectively). The γ-ray transitions belonging to ^{103}Rh were mainly identified from the excitation function data. Although γ-γ coincidence data were mainly used to construct the level scheme, they also helped in the identification of transitions which were in coincidence with known ^{103}Rh γ rays.[28,34]

The γ-γ-t coincidence measurements were carried out using standard techniques. Two Ge(Li) detectors were placed about 5 cm from the target at $\pm 90°$ with respect to the beam direction. Since many of the peaks in the singles spectrum represent more than one transition (see Fig. 2), good statistics were needed in the γ-γ coincidence spectra. About 3×10^7 coincidence events were recorded for off-line analysis. The three-parameter coincidence events were reduced with a program which provided a gain-corrected, symmetrized γ-γ coincidence matrix in a single scan of the data. The final coincidence matrix, which had dimensions of $3K \times 3K$, was stored in a triangular array. The advantage of processing data in this fashion is that all of the coincidence information available for each transition is obtained from a single coincidence spectrum. More than 300 gates were set on γ-ray transitions during the analysis. The background spectrum was produced by setting gates on more than 100 background regions throughout the spectrum. Figure 3 shows sample coincidence spectra for the positive and the negative parity bands. While these gates are not associated with the strongest lines in the coincidence spectrum, they are typical and reflect the general quality of the coincidence data.

Gamma-ray angular distribution spectra were taken at five angles between 90 and 150° relative to the beam axis. The spectra were normalized to well-resolved peaks from ^{103}Rh in a monitor detector located at 125° The data acquisition system provided a common dead time for both detectors, therefore eliminating the need for a relative dead time correction. Peak areas were extracted with a modified version of the program SAMPO.[35] Typical fits are shown in Fig. 2. To extract the angular distribution coefficients the normalized peak areas were fitted with the Legendre polynomial expansion

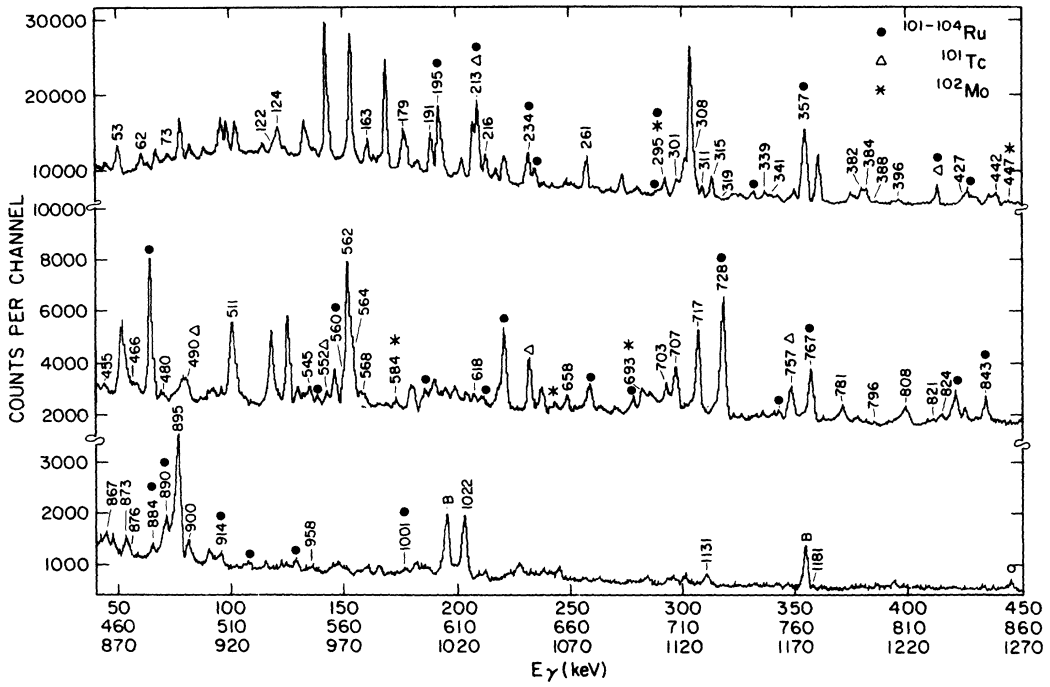

FIG. 1. Gamma-ray spectrum from the bombardment of ^{100}Mo with 45 MeV ^{7}Li.

$$W(\theta)=A_0+A_2P_2(\cos\theta)+A_4P_4(\cos\theta)\ ,$$

where θ is the angle with respect to the beam direction. The coefficients provide the change in the angular momentum, $|\Delta I|$, for the transitions, but do not give either the sign of ΔI or the parity change. However, these ambiguities can be resolved by appealing to the so-called yrast argument which states that the transitions observed in heavy ion reaction tend to follow $I_i=I_f+\Delta I$. This yrast argument is the strongest for the $\Delta I=2$ transitions.

III. EXPERIMENTAL RESULTS

The level scheme of ^{103}Rh deduced from the present data is shown in Fig. 4. It mainly consists of four well-developed bands and two weaker ones. The level scheme was constructed primarily from coincidence relationships. For some cascades the order of the transitions was determined from the intensities in the coincidence and the singles spectra. While the transition energies were used to confirm placement, no γ ray was placed in the level scheme solely on the basis of its energy. Each group in the level scheme will be discussed separately.

The experimental results for more than 70 γ-ray transitions assigned to ^{103}Rh are summarized in Table I. Column 1 lists the γ-ray energies. The relative intensities at 125° with respect to the beam direction are given in column 2. The angular distribution coefficients are shown in columns 3 and 4. The placement of the transitions is indicated in column 5. The intensities of several transitions have been corrected for overlap with lines from other exit channels. The nature of the contamination is noted in Table I.

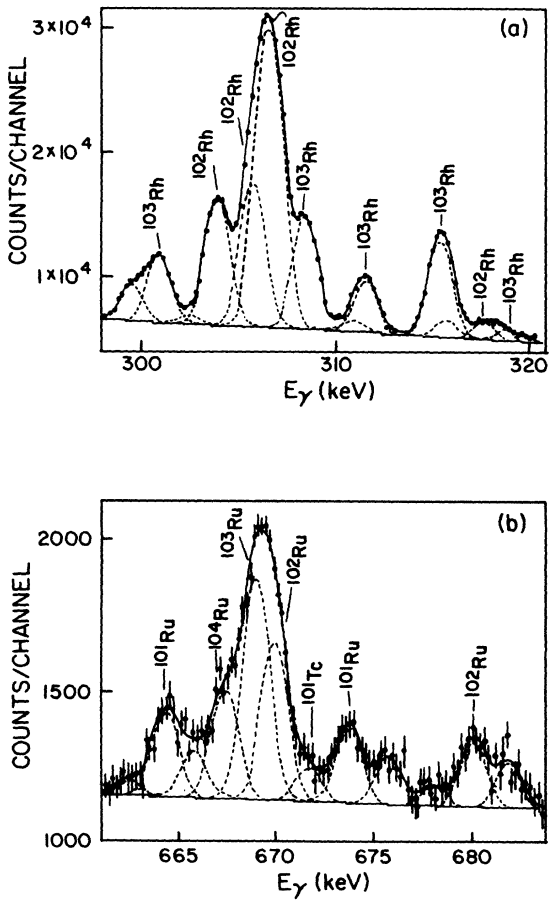

FIG. 2. Two regions of the singles spectrum for the ^{100}Mo(^{7}Li,4nγ) reaction fitted with the SAMPO program.

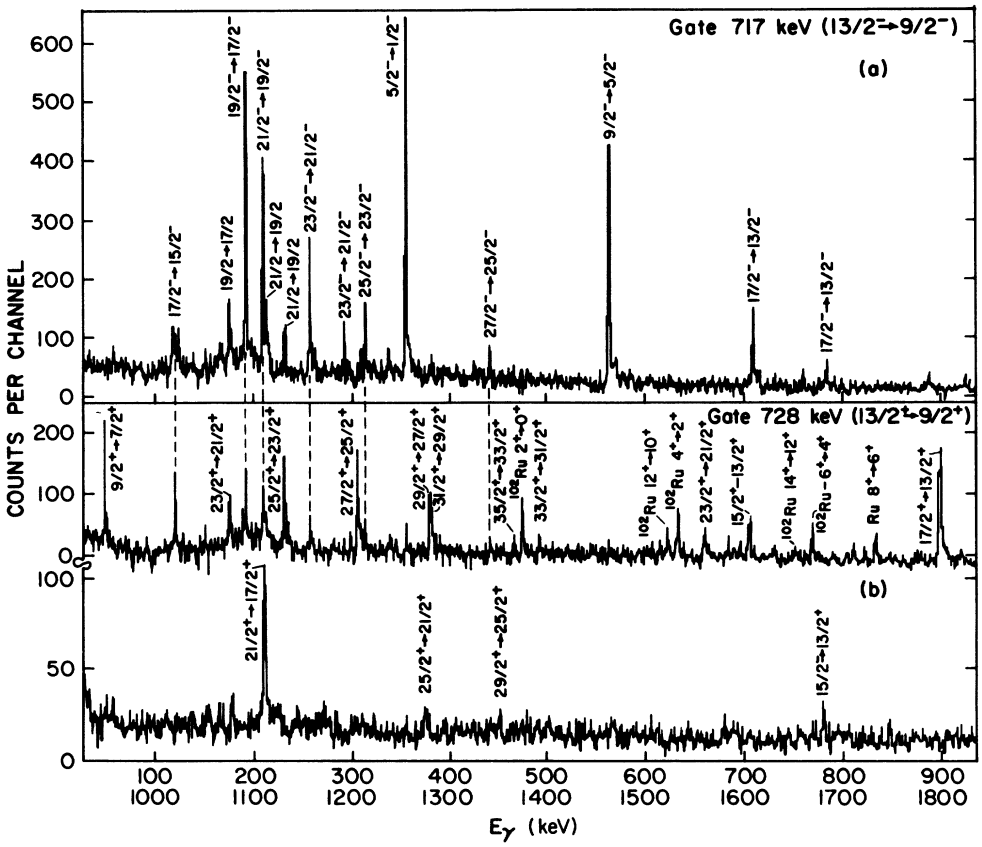

FIG. 3. Some examples of gated coincidence spectra for positive and negative parity bands. The spectra have been corrected for background contributions.

The two stretched $E2$ transitions at 357 and 563 keV which form the first part of a band based on the $\frac{1}{2}^-$ ground state were known previously from decay studies.[28,34] The extension of this band is firmly established by coincidence relationships with these two transitions [see Fig. 3(a)]. On the basis of angular distribution data, spin assignments of $\frac{5}{2}^-$, $\frac{9}{2}^-$, $\frac{13}{2}^-$, $\frac{17}{2}^-$, and $\frac{21}{2}^-$, were made for the 357-, 920-, 1638-, 2419-, and 3215-keV levels, respectively. The levels above $\frac{17}{2}^-$ in this negative parity band were not reported in Refs. 30 and 31.

A strong $\Delta I=1$ cascade based on the $(\frac{17}{2})^-$, 2346-keV level was identified. As shown in Figs. 3(a) and (b) this band is well established from γ-γ coincidences. The angular distribution data for the 707-keV γ-ray suggest $\Delta I=2$ for this transition ($\frac{17}{2}^- \rightarrow \frac{13}{2}^-$). The angular distributions of all the transitions deexciting this band (583, 707, and 821 keV) strongly support the assignment of negative parity to this band. The angular distribution data for interband transitions support the spin assignments of $\frac{19}{2}^-$, $\frac{21}{2}^-$, $\frac{23}{2}^-$, $\frac{25}{2}^-$, $\frac{27}{2}^-$, and $\frac{29}{2}^-$ for the 2541-, 2754-, 3015-, 3331-, 3772-, and 4340-keV levels, respectively. Except for the last transition this side band was also observed in Ref. 31.

Two other weak side bands which primarily feed the negative parity band were also observed with band heads at excitation energies of 2522 and 2936 keV, respectively. These bands are solidly based on coincidence relationships, as can be seen in Fig. 3. The quadrupole nature of the 884-keV transition agrees with the spin assignment of $\frac{17}{2}^-$ for the 2522 keV level. The angular distributions for the 179-, 216-, 312-, and 442-keV transitions are consistent with spin assignments of $\frac{19}{2}^-$, $\frac{21}{2}^-$, $\frac{23}{2}^-$, and $\frac{25}{2}^-$ for the 2702-, 2918-, 3230-, and 3672-keV levels, respectively. The deexcitation pattern of the 2522 keV level ($\frac{17}{2}^-$) indicates a negative parity assignment for this side band. The coincidence relationships for the other side band at 2936 keV can also be seen in Fig. 3. This part of the level scheme was reported in Ref. 31, but no spin assignments were made. None of the transitions from these two side bands were reported in Ref. 30.

A strong stretched $E2$ cascade was observed in coincidence with the 53 keV transition which deexcites the $\frac{9}{2}^+$ isomeric state ($t_{1/2}=1.1$ ns). A coincidence spectrum for this positive parity band is shown in Fig. 3(b). The quadrupole nature of the 728-, 895-, 1022-, and 1131-keV γ transitions established from the angular distributions yield spin assignments $\frac{13}{2}^+$, $\frac{17}{2}^+$, $\frac{21}{2}^+$, and $\frac{25}{2}^+$ for the 821-, 1717-, 2740-, and 3871-keV levels, respectively. The positive parity levels above $\frac{21}{2}$ were not previously reported in either of Ref. 30 or 31.

Another strong $\Delta I=1$ band is built on the $\frac{21}{2}^+$ state. This band, which is completely new, is solidly based on γ-γ coincidences [see Fig. 3(b)]. The angular distribu-

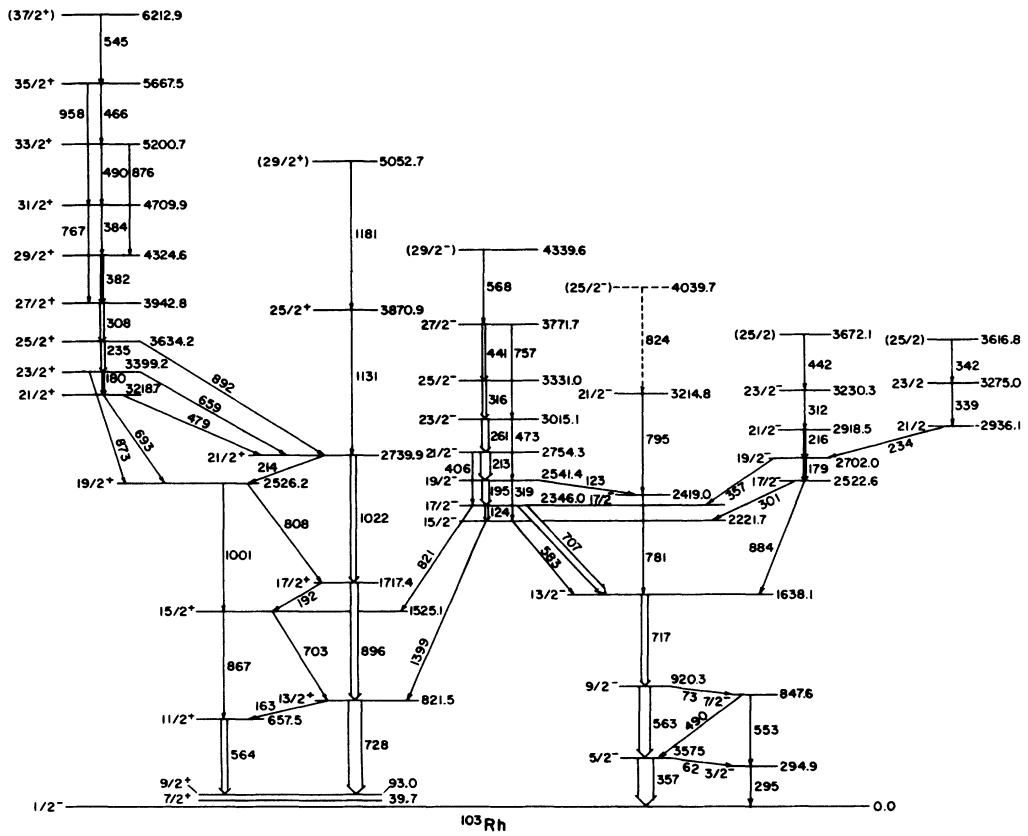

FIG. 4. Level scheme of ^{103}Rh. The dotted transition and level are considered probable, but were not definitely established by the data.

TABLE I. The γ-ray energies, intensities, and angular distribution coefficients for transitions assigned to ^{103}Rh following the ^{100}Mo(^{7}Li,4n) reaction at 45 MeV. The uncertainties in the energies (intensities) are 0.3 keV (10%) for strong transitions ($I_\gamma > 20$) and 0.5 keV (20%) for the weaker transitions. The intensities have been corrected for contamination for cases *b* and *c* (see below).

Energy (keV)	I_γ (rel)	A_2/A_0	A_4/A_0	Placement
53.3[a]		−0.22(7)		93→40
62.4[a]	5.4			357→295
73.5[a,b]	8.2	−0.33(9)	−0.03(2)	920→847
122.3	7.5	−0.28(10)	0.01(1)	2541→2419
124.4	19.5	−0.10(4)		2346→2221
163.5[a]	6.0	−0.16(6)		821→657
179.4[a]	28.4	−0.25(8)	−0.01(1)	2702→2522
180.5[a]	26.9	−0.19(5)	−0.02(1)	3399→3219
191.9	5.2			1717→1525
195.4[b]	71.8	−0.28(7)	−0.06(4)	2541→2346
212.9[b,c]	77.6	−0.26(6)	0.01(1)	2754→2541
214.0	5.2			2740→2526
216.5[a,b]	22.8	−0.23(8)		2918→2702
234.1[b]	21.5			2936→2702
235.0[b]	31.0	−0.06(4)		3534→3399
260.9[a,b]	49.5	−0.25(8)	0.07(5)	3015→2754
294.9[b,c]	18.7	−0.33(7)		295→0
301.0[a]	23.9			2522→2221
308.6[a]	30.5	−0.32(4)		3943→3634
311.8	6.7	−0.32(6)	−0.03(1)	3230→2918
315.9	34.8	−0.16(3)	0.10(5)	3331→3015
319.7	1.9			2541→2221
339.9[a]	10.4	−0.13(6)		3275→2936

TABLE I. (*Continued*).

Energy (keV)	I_γ (rel)	A_2/A_0	A_4/A_0	Placement
341.8	10.3	−0.29(7)		3617→3275
357.5[b]	142.2	0.27(3)	−0.08(6)	357→0
382.3	22.1	−0.17(6)		4324→3943
384.9[a]	19.1	−0.24(3)		4710→4324
396.5[a]	5.3			
406.5	1.0			2754→2346
427.5[a,b]	17.4			
440.7[a]	17.0	−0.33(7)		3772→3331
441.8[a]	16.4	−0.13(1)		3672→3230
447.5[a]	8.3			
455.6[a]	6.5			
466.8[a]	6.3	−0.48(7)	−0.03(2)	5667→5201
473.2[b]	7.8			3015→2541
479.8	3.6			3219→2740
490.8[c]	13.4	−0.29(7)	0.01(1)	5201→4710
				847→357
545.4	13.7	−0.29(7)	0.03(1)	6213→5667
552.7[c]	9.5	0.10(5)	−0.31(6)	847→295
562.8	104.0	0.25(3)	−0.20(9)	920→357
564.5	46.5	−0.07(4)		657→93
567.9[a]	8.8	−0.07(6)	0.02(1)	4339→3772
583.6[c]	10.9	−0.11(4)		2221→1638
618.5[a]	6.5			657→40
659.2[a]	15.8	−0.23(6)	0.09(6)	3399→2740
692.6[c]	17.5			3219→2526
703.6	18.7			1525→821
707.9	42.0	0.31(5)	−0.02(1)	2346→1638
717.8	77.3	0.36(5)	−0.01(1)	1638→920
728.6[b]	100.0	0.29(7)	−0.06(5)	821→93
756.8[c]	4.5			3772→3015
767.1[c]	4.2			4710→3943
780.9[a]	17.7	0.25(6)	−0.13(10)	2419→1638
795.8	1.3			3215→2419
808.9	15.8	−0.16(4)		2526→1717
821.0	6.2	−0.27(1)		2346→1525
824.9	10.5	0.27(5)		4040→3215
867.3	10.3	0.26(8)		1525→657
873.2	10.3	0.14(6)		3399→2526
876.5	1.5			5201→4325
884.2	6.4	0.29(8)	−0.16(9)	2522→1638
892.9	15.3	0.13(2)		3634→2740
895.9	74.8	0.11(1)	−0.10(8)	1717→821
900.2[a]	13.1			
914.1[a]	7.6			
958.3	1.8			5667→4710
1000.8	8.2			2526→1525
1022.5	36.3	0.17(2)	−0.19(12)	2740→1717
1131.0	3.7	0.10(8)		3871→2740
1181.8	2.7			5053→3871
1399.6	10.2			2221→821

[a]Contamination from ^{102}Rh.
[b]Contamination from $^{101-104}$Ru.
[c]Mixed with transitions from ^{101}Tc or ^{102}Mo.

tion coefficient of the 659- and 873-keV transitions, as well as the feeding pattern and deexcitation paths of this side band are in agreement with a positive parity and spin assignment of $\frac{23}{2}$ for the 3399-keV level. The angular distribution of the 180 keV transition is in agreement with the spin assignment of $\frac{21}{2}^+$ for the 3219 keV level. The angular distributions of the other transitions in this band agree with the spin assignments of $\frac{25}{2}^+$, $\frac{27}{2}^+$, $\frac{29}{2}^+$,

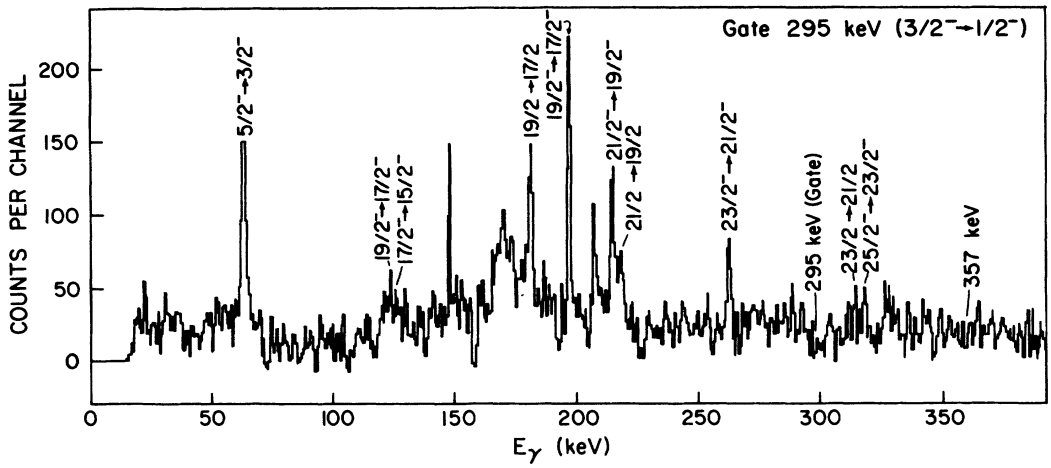

FIG. 5. Coincidence spectrum gated by the 295 keV transition.

$\frac{31}{2}^+$, $\frac{33}{2}^+$, $\frac{35}{2}^+$, and $\frac{37}{2}^+$ for the 3634-, 3943-, 4325-, 4710-, 5201-, 5667-, and 6213-keV levels, respectively.

Besides showing a new, well-developed, high-spin band, the current data extend to higher spins than observed in previous work.[30,31] There are not any major disagreements with Ref. 31 except for one level and the placement of one transition. Our data do not confirm the existence of the 3048 keV level and the placement of a second 295 keV transition. According to Charvet *et al.*[31] this transition was found to be in coincidence with itself and also with the 357 keV transition. The present data do not support this, as can be seen in Fig. 5, which shows the coincidence spectrum gated by the 295 keV transition.

In the work of Kajrys *et al.*,[30] only 25 transitions were assigned to ^{103}Rh and placed in the level scheme. The two transitions (497- and 863-keV) placed in the positive parity band feeding the 40- and 657-keV levels were not observed in the current work. A major discrepancy with Ref. 30 occurs in the spin assignment of $\frac{3}{2}^-$ to the 847 keV level. The coincidence relationship observed between the 73 keV transition and the 717-, 553-, and 490-keV transitions rule out a $\frac{3}{2}^-$ spin assignment for this level.

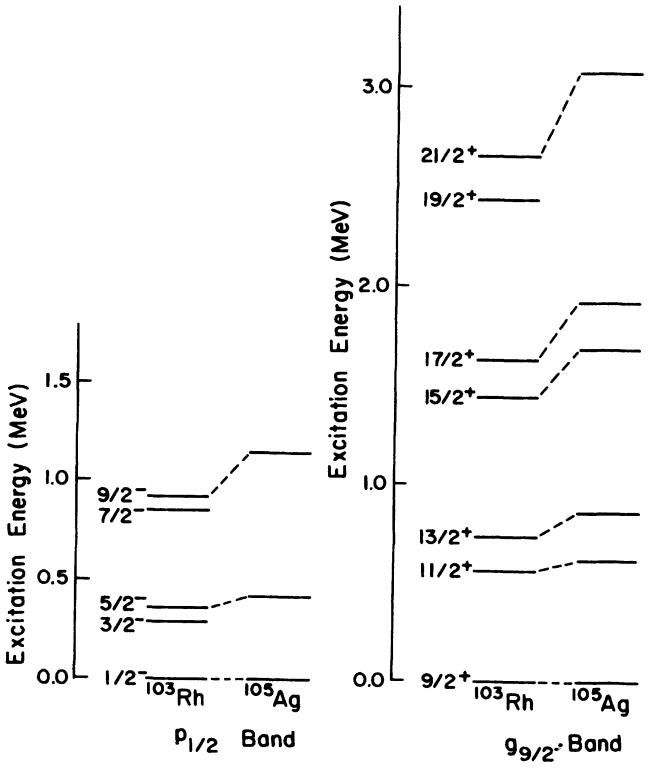

FIG. 6. Comparison of positive and negative parity bands in ^{105}Ag and ^{103}Rh. The ^{105}Ag data are taken from Ref. 9.

IV. DISCUSSION

The complex level scheme of ^{103}Rh will be divided into two parts for purposes of discussion. The low lying collective bands based on one quasiproton configurations (both positive and negative parity) will be described using a variety of different models: the symmetric rotor, the generalized asymmetric rotor, and the IBFM. The bands at higher excitation energies based on three quasiparticle (qp) configurations will be interpreted in terms of the cranked shell model. Most of these model comparisons suggest a configuration dependent deformation in ^{103}Rh.

A. Interpretation of 1qp configurations

1. Rotational description

The rotational-like behavior of the odd-A Ag isotopes in the mass 100 region has been interpreted with the symmetric rotor model.[9] Because of the similarity of ^{105}Ag and ^{103}Rh (see Fig. 6) the application of the symmetric rotor model to ^{103}Rh data seems quite reasonable. This model is based on a slightly deformed symmetric core with Coriolis interactions. A variable moment of inertia (VMI) accounts for the softness of the core. This model, which is described in detail in Ref. 8, originally assumed a rigid rotor core. In this form it was applied to well deformed nuclei in the rare-earth region[36,37] where it reproduced the experimental results quite well.

The parameters involved in the calculation are κ and μ of the Nilsson model, the deformation ε_2, the pairing parameter Δ and the Fermi surface λ_f. The VMI parameters consist of the ground state moment of inertia, $\mathcal{J}_0$, and the stiffness, C. Most of the parameters were kept constant throughout the calculations. The parameters were determined according to the following prescription. The values of the Nilsson parameters ($\kappa=0.069$ and $\mu=0.43$) were chosen to give the best fit to the energy levels at zero deformation as determined by Reehal and Sorensen.[38] This choice also agrees with the interpolation between heavy and light mass regions proposed by Larsson *et al.*[39] A Nilsson diagram for the $N=3,4$ proton shells is shown in Fig. 7 for the above values of κ and μ. The pairing energy, $\Delta=1.5$ MeV, was calculated from empirical mass differences as described by Bohr and Mottelson.[40] The Fermi surface in this calculation was placed between the $\frac{1}{2}$[301] and the $\frac{7}{2}$[413] proton orbitals to preserve the number of particles (see Fig. 7). The VMI parameter $\mathcal{J}_0$ was set equal to zero as assumed in Pd and Ag calculations.[8,9] The value $C=6.0\times10^{-3}$ MeV^3 was calculated using the formalism described by Mariscotti *et al.*,[41] using an average ^{102}Ru and ^{104}Pd core. Coriolis matrix elements were attenuated by factor of 0.7 in accord with calculations for Pd and Ag.[8,9] This attenuation is necessary to reproduce the experimental data even in strongly deformed nuclei.[36] The deformation parameter ε_2 was adjusted to give the best fits to the experimental energy levels and the transition probabilities.

The calculations for the negative-parity band included the Nilsson states from the $2p_{1/2}$, $2p_{3/2}$, and $1f_{5/2}$ orbitals. The states from the $1f_{7/2}$ orbital were excluded since their contribution to the mixing amplitude is negligible. Table II shows the basis states used in these calculations along with their energies, quasiparticle energies, and occupation probabilities. The above parameters with a deformation of $\varepsilon_2=0.2$ ($\beta=0.21$) provide a good fit to the experimental data for the $2p_{1/2}$ band (see Fig. 8). The calculations for positive-parity states included Nilsson states from the unique parity ($1g_{9/2}$) orbital. With the above parameters and the proper Fermi surface λ_f, no value of ε_2 could generate a reasonable fit to the experimental data for the $1g_{9/2}$ band. Figure 9 shows a comparison between the experimental and the calculated positive parity levels.

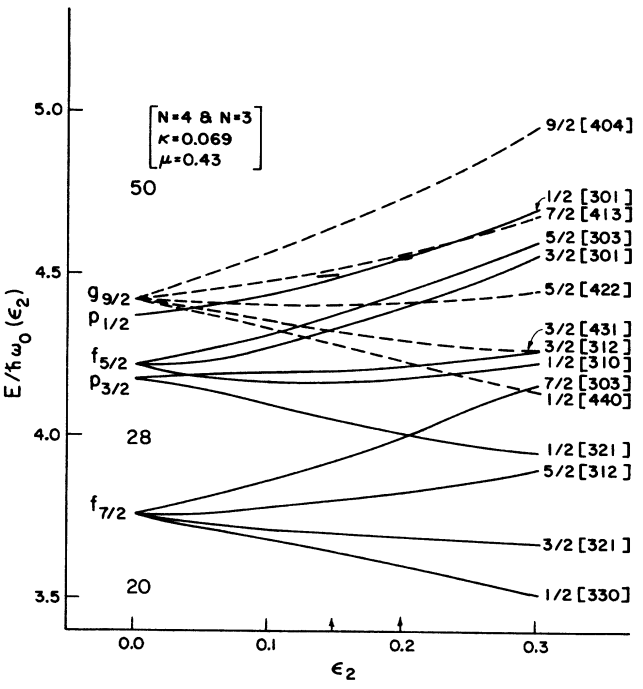

FIG. 7. Nilsson diagram for Rh ($Z<50$). The Fermi surfaces for two different values of the deformation are shown with solid lines.

Since both the deformation and the VMI parameter (C) are related to the core, it seems appropriate to fit the $1g_{9/2}$ band treating both ε_2 and C as free parameters. By keeping the other parameters constant while maintaining the proper Fermi surface, better agreement between the experimental and the calculated values could be obtained by decreasing ε_2 and increasing C. The values $\varepsilon_2=0.15$ ($\beta=0.16$) and $C=2.0\times10^{-2}$ MeV^3, gave the best fit to the experimental energy level for the $1g_{9/2}$ band (see Fig. 9). The small deformation and larger stiffness strongly suggest that the nucleus becomes more spherical when the odd proton occupies the $1g_{9/2}$ orbital. Since no experimental $B(E2)$ values are known for the $g_{9/2}$ band, the accuracy of ε_2 obtained from the fit cannot be determined. However, the fact that C must be increased to fit the $1g_{9/2}$ band is consistent with the above statement. Some discrepancies still remain between theory and experiment. As in the ^{105}Ag calculations,[9] this model predicts a low-lying $\frac{7}{2}^+$ state, but it lies above the $\frac{9}{2}^+$ (see Table III). For the odd-A Rh and Ag isotopes Paar[42] has shown that the coupling of a 3 proton hole cluster can shift the $\frac{7}{2}^+$ state below the $\frac{9}{2}^+$ state. Recently, Heyde and Paar[43] pointed out that calculations with the cluster vibrator model, the interacting boson-fermion model and the Nilsson model provide an explanation for the low-lying $\frac{7}{2}^+$ level using a quadru-

TABLE II. Nilsson states used as basis states in the Coriolis calculations, and their related energies and occupation probabilities. The parameters used are given in the text.

Nilsson state	Energy e (MeV)	qp energy e' (MeV)	Occupation probability v^2
$\frac{1}{2}^-$[301]	−0.06	0.001	0.519
$\frac{1}{2}^-$[310]	−3.41	2.223	0.958
$\frac{1}{2}^-$[321]	−5.00	3.717	0.978
$\frac{3}{2}^-$[301]	−1.42	0.567	0.844
$\frac{3}{2}^-$[312]	−3.11	1.957	0.950
$\frac{5}{2}^-$[303]	−1.01	0.310	0.779
$\frac{1}{2}^+$[440]	−2.04	1.036	0.902
$\frac{3}{2}^+$[431]	−1.64	0.722	0.868
$\frac{5}{2}^+$[422]	−0.91	0.256	0.760
$\frac{7}{2}^+$[413]	0.07	0.002	0.476
$\frac{9}{2}^+$[404]	1.27	0.467	0.176

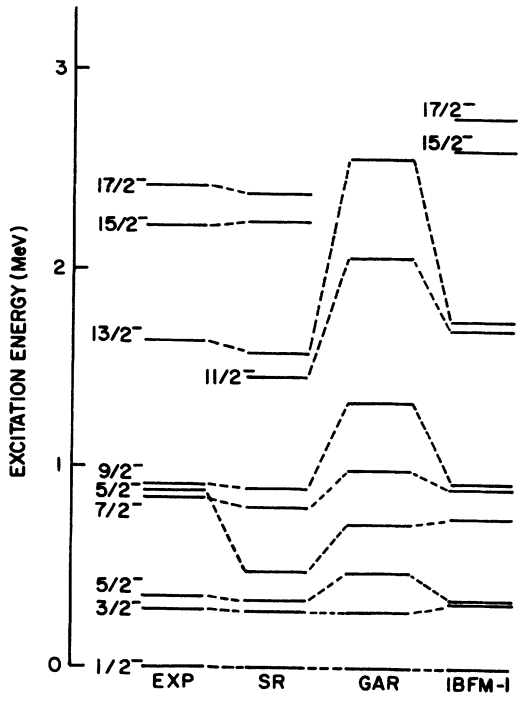

FIG. 8. Comparison of the experimental energy levels with the predictions of the symmetric rotor model (SR), generalized asymmetric rotor (GAR), and interacting boson-fermion model (IBFM-1) for the $\pi p_{1/2}$ band in ^{103}Rh.

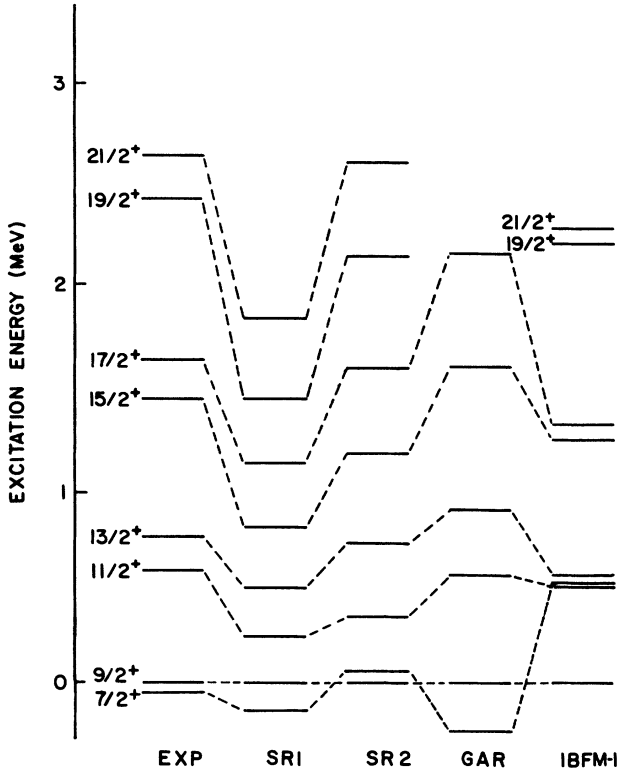

FIG. 9. Comparison of the experimental energy levels with the predictions of different models for the $\pi g_{9/2}$ band in ^{103}Rh. The models are the same as in Fig. 8; SR1 and SR2 refer to symmetric rotor model calculations with different deformation parameters (see text for details).

pole residual interaction.

The experimental and the calculated energy levels for the positive and the negative parity bands are given in Table III, along with the wave functions of the states in terms of the basis states. As can be seen from Table III, the negative parity band shows very little mixing of basis states for the ground state and excited states, $\frac{1}{2}$[301] being the major component of the wave function. This is characteristic of a decoupled band as is reflected in the decoupling parameter of 0.86. The results in Table III show a large amount of Coriolis mixing for the unique parity orbital. For this band the Fermi surface lies near the high j orbitals ($K=\frac{7}{2},\frac{9}{2}$) and has a $\Delta I=1$ spin sequence with large signature splitting. This indicates an intermediate coupling, a coupling between strongly occupied and decoupled limits.[44] The overall agreement between the calculated and experimental energy levels is good.

In addition to energy level calculations, the electromagnetic properties of the transitions give further insight into the structure of ^{103}Rh. The electric and magnetic multipole expansion for this model has been discussed in detail in Refs. 8 and 9. No free parameters were used to calculate the transition probabilities. The $B(E)2$'s predicted by this calculation are compared with experimental results[28] in Table IV. The calculated and the experimental $B(E2)$'s are in reasonable agreement except for transitions from the $\frac{7}{2}^-$ and the second $\frac{5}{2}^-$ levels. The discrepancy might arise from the fact that the symmetric rotor model does not include the quasi-β band in the collective motion. In other words, the set of wave functions used in the symmetric rotor calculation is not a complete set as far as the quasi-β band is concerned. This was shown to be important for the Pd isotopes in Ref. 45. The experimental and the calculated branching ratios are compared in Table V.

By applying the symmetric rotor model to different quasiproton configurations in the same nucleus, one would expect that the same core parameters and Coriolis interactions should account for all the observed differences between the bands. This does not seem to be the case in ^{103}Rh. The results of these calculations are consistent with the idea of configuration dependence deformation. This point was not explored in Ref. 9 since the $2p_{1/2}$ band was not as strongly populated for the Ag isotopes and, therefore, the difference between the $1g_{9/2}$ and the $2p_{1/2}$ bands were not as apparent as in the ^{103}Rh case (see Fig. 6).

2. *Asymmetric description*

As mentioned earlier, potential energy surface calculations for some of the isotopes in the mass 100 region predict symmetric prolate, oblate, and also triaxial, shapes. The generalized particle-asymmetric rotor model has been used to describe the negative parity band in

TABLE III. Summary of energy levels and wave functions from the Coriolis calculations.

I	Energy exp.	(keV) calculated	Coriolis mixing, f_{IK}^2 (amplitude)^2					
			Positive-parity states					
			$\frac{1}{2}$[440]	$\frac{3}{2}$[431]	$\frac{5}{2}$[422]	$\frac{7}{2}$[413]	$\frac{9}{2}$[404]	
	n-even states							
$\frac{9}{2}$	0	0	0.004	0.020	0.123	0.445	0.408	
$\frac{13}{2}$	728	701	0.022	0.067	0.237	0.465	0.208	
$\frac{17}{2}$	1624	1586	0.056	0.123	0.299	0.399	0.122	
$\frac{21}{2}$	2646	2609	0.103	0.174	0.322	0.328	0.078	
$\frac{25}{2}$	3777	3752	0.138	0.214	0.325	0.269	0.053	
$\frac{29}{2}$	4959	5001	0.175	0.243	0.319	0.225	0.038	
	n-odd states							
$\frac{7}{2}$	−53	60	0.002	0.032	0.232	0.734		
$\frac{11}{2}$	564	330	0.002	0.031	0.181	0.490	0.296	
$\frac{15}{2}$	1431	1153	0.005	0.064	0.266	0.480	0.184	
$\frac{19}{2}$	2432	2141	0.008	0.095	0.320	0.446	0.130	
	other states							
$\frac{5}{2}$	497	542	0.079	0.231	0.690			
			Negative-parity states					
			$\frac{1}{2}$[301]	$\frac{1}{2}$[310]	$\frac{1}{2}$[321]	$\frac{3}{2}$[301]	$\frac{3}{2}$[312]	$\frac{5}{3}$[303]
	n-even states							
$\frac{1}{2}$	0	0	0.998	0.000	0.002			
$\frac{5}{2}$	357	337	0.994	0.000	0.001	0.000	0.003	0.002
$\frac{9}{2}$	920	895	0.984	0.003	0.000	0.000	0.006	0.007
$\frac{13}{2}$	1638	1586	0.970	0.004	0.000	0.000	0.007	0.017
$\frac{17}{2}$	2419	2376	0.948	0.006	0.000	0.001	0.013	0.032
$\frac{21}{2}$	3215	3247	0.912	0.008	0.000	0.004	0.018	0.058
$\frac{25}{2}$	4040	4185	0.859	0.011	0.000	0.008	0.026	0.096
	n-odd states							
$\frac{3}{2}$	295	284	0.992	0.002	0.000	0.004	0.001	
$\frac{7}{2}$	847	804	0.976	0.006	0.000	0.012	0.003	0.003
$\frac{11}{2}$		1467	0.964	0.008	0.000	0.022	0.004	0.002
$\frac{15}{2}$	2222	2236	0.949	0.013	0.000	0.032	0.006	0.000
$\frac{19}{2}$		3088	0.931	0.016	0.000	0.045	0.008	0.000

the $^{105-109}$Ag isotopes.[10] The low-lying levels of $^{105-109}$Ag have been fitted with an asymmetric core having $\varepsilon_2=0.26$ and $\gamma=32°$. The agreement with the data was found to be as good as that obtained with the symmetric rotor model. Recently, the g factors of the ^{107,109}Ag have been measured by the perturbed angular correlation, transient field technique. The results were compared with a weak coupling calculation and Nilsson model calculations with either a symmetric or a triaxial core.[46] The authors showed that the correct sign of the quadrupole and the value of the g factor for these nuclei (^{107,109}Ag) were best predicted by the asymmetric rotor model with the deformation parameters $\varepsilon=0.26$, $\gamma=20°-24°$ (a change towards prolate from the previous calculation). This choice of the parameters did not give as good a fit to the energy levels as previous calculations but resulted in better agreement with the experimental electromagnetic properties.

In order to investigate the structure of ^{103}Rh in more detail, the generalized particle-asymmetric rotor model has been applied to this nucleus. A detailed description of the model can be found elsewhere.[47] In this model the deformation parameters are β and γ. The calculations of the negative parity band included the deformed basis of $2p_{1/2}$, $2p_{3/2}$, and $1f_{5/2}$ with mixing between these orbitals. The calculation for positive parity states

TABLE IV. Comparison of experimental and theoretical $B(E2)$'s.

E_1 (keV)	E_γ (keV)	$I_i \rightarrow I_f$	$B(E2, I_i \rightarrow I_f)\ e^2b^2$ Exp.	SR	GAR	IBFM-1
295	295	$\frac{3}{2} \rightarrow \frac{1}{2}$	0.109	0.134	0.104	0.110
357	357	$\frac{5}{2} \rightarrow \frac{1}{2}$	0.131	0.134	0.122	0.110
880	523	$\frac{5}{2}' \rightarrow \frac{3}{2}$	0.015	0.002		0.018
			0.225		0.154	
	586	$\frac{5}{2}' \rightarrow \frac{3}{2}$	0.007	0.003		0.006
			0.077		0.049	
	880	$\frac{5}{2}' \rightarrow \frac{1}{2}$	0.0044	0.001	0.035	0.000
847	490	$\frac{7}{2} \rightarrow \frac{5}{2}$	0.015	0.0006	0.015	0.000
	553	$\frac{7}{2} \rightarrow \frac{3}{2}$	0.130	0.001	0.164	0.136
920	563	$\frac{9}{2} \rightarrow \frac{5}{2}$	0.181	0.194	0.189	0.151

included the deformed basis from the unique parity ($1g_{9/2}$) orbitals. Both positive and negative parity states were calculated with the same deformation parameters. In these calculations we employed a large quadrupole deformation $\varepsilon_2=0.26$, a value close to the quadrupole deformation extracted from the first excited 2_1^+ states of ^{102}Ru ($\beta=0.24$),[15] which was chosen as a core. Coriolis matrix elements were attenuated by a factor of 0.7 as in the symmetric rotor case. The best fit to the experimental energy levels and the electromagnetic properties was obtained with deformation parameters of $\varepsilon_2=0.26$ and $\gamma=24°$. The results for the energy levels are compared in Figs. 8 and 9 for negative and positive parity bands, respectively. The overall agreement between calculated and experimental level energies is reasonable for a few low-lying levels in each band. The addition of a variable moment of inertia might improve the fit to the high-spin states. The calculated $B(E2)$'s for the negative parity band are given in Table IV. The agreement with the experimental results is quite good. This indicates that the set of the wave functions and the deformation parameters used in this model are a reasonable choice for the negative parity band in ^{103}Rh. Larger γ values improve the fit to the energy levels for the negative parity band, but result in a larger disagreement with the $B(E2)$'s. The asymmetric rotor's predictions of the energy levels are not as good as those of the symmetric rotor model. The signature splitting predicted by this model is also different from experimental values, which indicate that the actual core parameters are different than the values predicted by the model. Since no $B(E2)$'s are known for the positive parity band, it is difficult to determine the accuracy of the deformation parameters for the positive parity band. The difference between this model calculation and the previous symmetric rotor calculation is that the same core parameters resulted in reasonable fit to the energy levels for both bands.

TABLE V. Branching ratios in ^{103}Rh.

I_i	I_f	E_γ (keV)	Branching ratios Exp.	SR
$\frac{13}{2}^+$	$\frac{9}{2}^+$	728	0.94	0.99
	$\frac{11}{2}^+$	163	0.06	0.01
$\frac{15}{2}^+$	$\frac{11}{2}^+$	867	0.69	0.71
	$\frac{13}{2}^+$	703	0.31	0.29
$\frac{17}{2}^+$	$\frac{13}{2}^+$	896	0.91	0.00
	$\frac{15}{2}^+$	192	0.09	1.00
$\frac{19}{2}^+$	$\frac{15}{2}^+$	1001	0.34	0.85
	$\frac{17}{2}^+$	808	0.66	0.15
$\frac{21}{2}^+$	$\frac{17}{2}^+$	1022	0.87	1.00
	$\frac{19}{2}^+$	214	0.12	0.00
$\frac{5}{2}^-$	$\frac{1}{2}^-$	357	0.97	1.00
	$\frac{3}{2}^-$	62	0.03	0.00
$\frac{7}{2}^-$	$\frac{3}{2}^-$	553	0.41	0.28
	$\frac{5}{2}^-$	490	0.59	0.72
$\frac{9}{2}^-$	$\frac{5}{2}^-$	563	0.93	1.00
	$\frac{7}{2}^-$	73	0.07	0.00
$\frac{15}{2}^-$	$\frac{13}{2}^-$	584	0.44	0.77
	$\frac{13}{2}^+$	1399	0.56	0.23

3. *IBFM-1 calculation*

The interacting boson-fermion model[12,48] has been successful in describing low-lying collective excitations in heavy and medium heavy nuclei. Recently, the interacting boson fermion model (IBFM-1) has been applied to the odd-A Rh isotopes.[49] Both positive and negative parity states have been calculated with the same core parameters. In the IBFM-1, fermions in shell model orbitals of spin j are coupled to an even-even core. In this case, the ^{104}Pd core is described by IBM-1 (which does not distinguish between neutron and proton bosons) while the odd proton hole occupies a $1g_{9/2}$, $2p_{1/2}$, $2p_{3/2}$, or $1f_{5/2}$ orbital. In Ref. 49 the $2d_{5/2}$ orbital was also included, but this was not done in the current work since its effect on the energy levels and the $B(E2)$'s is negligible for this case. The advantage of using this

model is that the boson-fermion interaction term can describe all limiting cases including weak, strong, and intermediate coupling as well.

For many j shell cases, a large number of parameters are involved. For a unique parity case (single j shell), however, there is a great reduction in the number of parameters. The parameters and the semimicroscopic approach used to reduce the number of parameters is given in Ref. 49. This approach is different from that used to fit the Tc isotopes.[50] The results for the energy levels are compared in Figs. 8 and 9 for negative and positive parity bands, respectively. The overall agreement between calculated and experimental level energies is good up to $\frac{17}{2}^-$ for the negative parity band. Since the model considers only S and D bosons, the deviation for high-spin states is expected. The addition of G bosons might improve the agreement with high-spin states. However, these high-spin states show effects from band crossing which are not accounted for within the framework of the IBFM-1 model.

The calculated $B(E2)$'s are given in Table IV. The agreement with the experimental results is quite good even for transitions from the $\frac{7}{2}^-$ and the second $\frac{5}{2}^-$ levels. This indicates that the set of wave functions used by IBFM-1 is more complete than those used in the symmetric rotor calculation. The asymmetric rotor and IBFM-1 are equally successful in predicting the $B(E2)$ values for the negative parity band. The positive-parity band was fitted with the same core parameters. A comparison with the experimental results is shown in Fig. 9. Although the agreement with the experimental results is reasonable, the calculations for the $g_{9/2}$ band consistently underestimate the experimental level energies up to $\frac{21}{2}^+$. This indicates a possible change in the core, as suggested by the symmetric rotor results. Both models predict a similar behavior for the configurations involved.

The Pd isotopes represent a possible $SU(5)\rightarrow O(6)$ transition.[11] In the IBFM-1 this involves a transition from a particle-vibration-coupled $[SU(5)\times 1g_{9/2}]$ towards a γ-unstable rotor plus particle $[O(6)\times 1g_{9/2}]$. Using this interpretation (considering the ^{104}Pd was chosen as core in the IBFM-1 calculation) both IBFM-1 and asymmetric rotor calculations support the possibility of the γ softness in this nucleus.

4. *Possible interpretation for 1qp configurations*

As described above the symmetric rotor and IBFM-1 models predict the $\pi p_{1/2}$ band very well by using the even-even neighboring nucleus as a core, but the same core parameters cannot predict the energy levels of the unique parity orbital and the $p_{1/2}$ band simultaneously. Changes in the core parameters improved the fit to the data for the $\pi g_{9/2}$ band in the symmetric rotor model. One can qualitatively explain the difference between the $1g_{9/2}$ and $2p_{1/2}$ bands in ^{103}Rh in terms of the n-p interaction. Federman and Pittel[1,2] demonstrated that the n-p interaction was responsible for the sudden onset of deformation in Zr and Mo isotopes at $N=60$. Since the deformation arises from a few valence nucleons, an explicit shell model calculation was possible. Federman and Pittel[1,2] carried this out and predicted the shape transition. The strength of the n-p interaction is largest and therefore most effective in inducing deformation when the particles are in SOP orbitals with large spatial overlap. In orbitals such as the $\pi g_{9/2}$ and the $\nu g_{7/2}$ the n-p forces effectively cancel the driving force towards spherical shapes due to the n-n and p-p pairing correlations. For ^{103}Rh the change in energy obtained by maximizing the n-p interaction in SOP orbitals ($\pi g_{9/2}$, $\nu g_{7/2}$) should be compared with the change in the single particle and the pairing energies. The fact that the strength of the n-p interaction is different for the $g_{9/2}$ and $p_{1/2}$ orbitals in this region supports the idea of configuration dependent deformations. The size of the effect, however, is not clear since most models do not explicitly include the n-p interaction. Therefore, it is difficult to verify this quantitatively. According to recent developments in connecting the n-p interaction strength to the product of the number of valence protons and neutrons,[51] a qualitative explanation is possible. This will be discussed elsewhere in detail.[52]

B. Interpretation of 3qp configurations

1. *High-spin states*

Relatively little information is available on high-spin states in the mass 100 region. Recently Haenni *et al.*[26] have reported the first set of blocking experiments for ^{102}Ru. Data for ^{101,102,103}Ru and ^{101}Tc were obtained using massive transfer reactions. In ^{101,103}Ru the backbend in the $\nu h_{11/2}$ band is blocked (the data for ^{101}Tc are inconclusive). The current results for ^{103}Rh provide a more complete picture. The $\pi p_{1/2}$ band in ^{103}Rh shows an upbend at the same frequency as the backbend in ^{102}Ru. However, at first glance the backbend also seems to be blocked in the $\pi g_{9/2}$ band. In order to discuss the results for this nucleus, the band crossing has to be considered in more detail.

When two rotational bands cross at a fixed spin, the yrast line of the nucleus changes its intrinsic structure. A band crossing occurs at spin $\frac{21}{2}^+$ in the ^{103}Rh yrast line as the nucleus changes from $\pi g_{9/2}$ to 3qp configurations $[\pi g_{9/2}, \nu(h_{11/2})^2]_{21/2}$. Drastic changes in the band structure are expected after this crossing. Indeed, this seems to be the case in ^{103}Rh as well as in ^{107}Ag. For these nuclei the proton and neutron Fermi surfaces λ_p and λ_n always lie in different parts of their respective intruder j shells, therefore a configuration dependence of γ is expected. The reason lies in the fact that for transitional nuclei the restoring force of the quasiparticle vacuum (collective core) is comparable to or smaller than the quasiparticle forces.[25] Frauendorf suggests that the large signature splitting of the $\pi g_{9/2}$ band in ^{107}Ag and the disappearance of the splitting in the 3qp band are consequences of a shape change. A large negative γ deformation is associated with 1qp configuration ($\pi g_{9/2}$) while $\gamma\approx 0$ for the 3qp configurations containing a pair of $h_{11/2}$ neutrons. This feature is predicted by the cranked shell model. Figure 10 shows the relevant quasiparticle Routhians for ^{103}Rh.

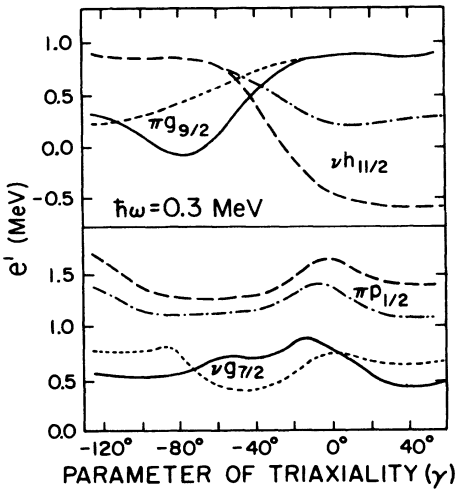

FIG. 10. Quasiparticle Routhians as a function of γ for the $Z=45, N\approx 58$ system at $\hbar\omega=0.3$ MeV and $\Delta_p=1.48$ MeV. The line convention is $(+,\frac{1}{2})$ solid, $(+,-\frac{1}{2})$ dotted, $(-,\frac{1}{2})$ long-dashed, $(-,-\frac{1}{2})$ short-dashed.

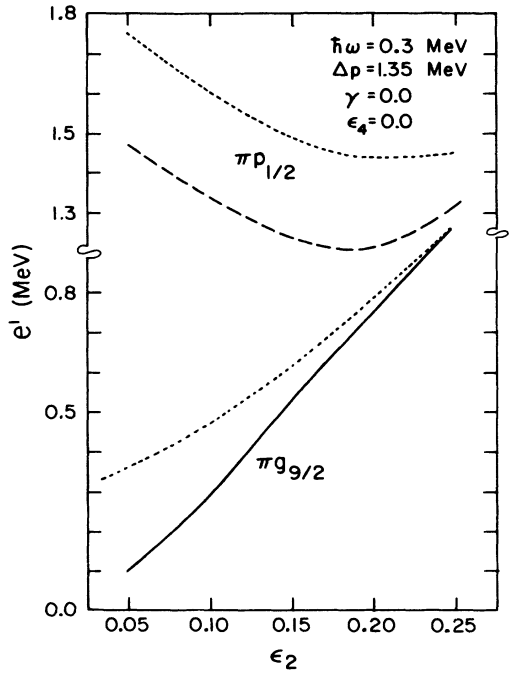

FIG. 11. Quasiparticle Routhians as a function of quadrupole deformation (ε_2) for ^{103}Rh. The parameters are given in the text. The line convention is $(+,\frac{1}{2})$ solid, $(+,-\frac{1}{2})$ lower-dotted, $(-,\frac{1}{2})$ long-dashed, $(-,-\frac{1}{2})$ upper-dotted.

Since there is j mixing, the j assignments are symbolic. The large signature splitting for the 1qp configuration $\pi g_{9/2}$ is related to large negative γ. The $h_{11/2}$ neutrons on the other hand have a large driving force toward positive γ values. Therefore, after the crossing, a pair of aligned $h_{11/2}$ neutrons pulls the protons toward $\gamma\approx 0$ where the signature splitting disappears (see Fig. 10). This interpretation of the positive parity high-spin states band shows that the $\pi g_{9/2}$ band in ^{103}Rh also backbends at the same frequency as ^{102}Ru.

The concept of configuration dependent triaxiality has also been successfully applied to the $A\approx 80$ and 160 regions,[24,23] where strong changes in γ are induced by quasiprotons in $g_{9/2}$ and $h_{11/2}$ orbitals and by quasineutrons in $g_{9/2}$ and $i_{13/2}$ orbitals. In the current work the configuration dependent deformation in ^{103}Rh is explored in a different way using the same model (CSM). Because of the softness of this nucleus, the quadrupole deformation is not well developed. Therefore, in the calculations ε_2 has been varied within reasonable limits. Figure 11 shows the Routhian as a function of quadrupole deformation. In this calculation the hexadecapole deformation was set equal to zero ($\varepsilon_4=0$). The proton pairing gap was reduced 15% from the experimental odd-even mass differences.[40] The frequency was fixed at 0.3 MeV/$\hbar$ and γ was set equal to zero. As it can be seen in Fig. 11, the signature splitting for the $\pi g_{9/2}$ band is large for small deformations but essentially disappears for $\varepsilon_2=0.2$. This indicates that for the $\pi g_{9/2}$ band it is not necessary to associate the shape change with a large change in γ. Perhaps, the deformation is smaller ($\varepsilon_2\approx 0.15$) for the 1qp excitation in ^{103}Rh and is larger ($\varepsilon_2=0.2$–0.25) for the 3qp configuration where the signature splitting disappears. The $\pi p_{1/2}$ band has a large positive signature splitting which is rather insensitive to γ and ε_2. Therefore, the large signature splitting of this band is not necessarily related to large γ deformation.

The enhancement of $M1$ transition probabilities above the crossing has been explained using the semiclassical approach of Donau.[53] According to Donau, in the rotating frame the rotation axis of the system is the total angular momentum I, which is different from I_x (aligned axis) for high-K bands. This allows the aligning particles to contribute coherently to the time dependent (perpendicular) component of the magnetic moment. The enhancement of $M1$ transition probabilities are partially due to the fact that the perpendicular moments of the particle in the $\pi g_{9/2}$ and the $\nu h_{11/2}$ orbitals add up and give a larger magnetic moment than the one before the alignment. Experimental data for the high-spin band based on the $\frac{21}{2}^+$ state in ^{103}Rh show a very small signature splitting and also show an enhancement of the $M1$ transition probabilities, as reflected by the increase in the $B(M1)/B(E2)$ ratios. Figure 12 shows these ratios before and after the crossing assuming that the $\Delta I=1$ transitions are pure $M1$. The geometrical approach of Donau was modified to include the effect of nonzero γ on the $E2$ rate.[23] The $B(M1)/B(E2)$ ratio is given by

$$\frac{B(M1;I\to I-1)}{B(E2;I\to I-2)}=\frac{12}{5Q_0^2\cos^2(30^\circ+\gamma)}\{(g_\pi-g_R)[(I^2-K^2)^{1/2}-i_\pi]-(g_\nu-g_R)i_\nu\}^2\frac{K^2}{I^2}\left[1-\frac{K^2}{(I-1/2)^2}\right]^{-2}.$$

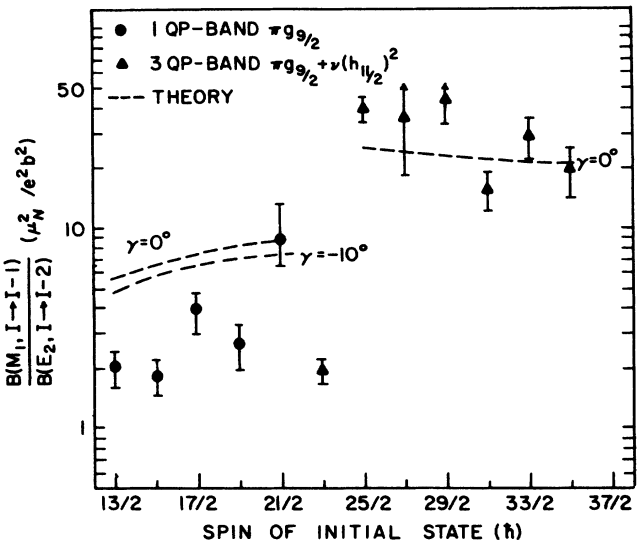

FIG. 12. Ratio of $M1$ to $E2$ transition probability for the $\pi g_{9/2}$ band. Experimental values come from observed branching ratios, and the theoretical values were obtained by using an equation given in Ref. 23. Theoretical parameters are given in the text.

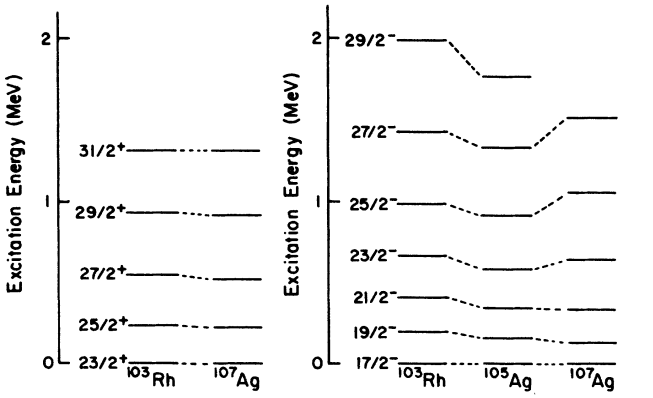

FIG. 13. Comparison of the relative excitation energies of negative $3qp$ configurations in ^{105}Ag and ^{103}Rh. Data for ^{105}Ag are taken from Ref. 9.

The calculation was performed using the values $K=\frac{7}{2}$, $(g_\pi - g_R)=0.88$, $(g_\nu - g_R)=-0.68$, $i_\pi=2.8\hbar$, and $i_\nu=7.6\hbar$. The value of Q_0 was taken from Ref. 15. The results of this calculation are also shown in Fig. 12. The experimental data show an enhancement of a factor of 20 after the crossing. The prediction from this semiclassical expression for the 1qp band with $\gamma=0°$ is shown in Fig. 12. The results overestimate the experimental $B(M1)/B(E2)$ ratios by factor of two. A large negative γ deformation ($\gamma=-50$ or $-10°$) decreases the estimated values of the $B(M1)/B(E2)$ ratio but cannot compensate for the large discrepancy (see Fig. 12). After the crossing the estimate from the above expression is in agreement with zero γ deformation for the 3qp band.

The high-spin states built on the yrast $\frac{17}{2}^-$ band head are more difficult to interpret. Similar bands have also been observed in ^{105,107}Ag. In Fig. 13 the relative excitation energies of negative $3qp$ configurations are compared for ^{103}Rh and ^{105}Ag. Frauendorf and Keller[25,54] interpreted the bands in the Ag isotopes as the three quasiparticle configuration $[\pi g_{9/2}, \nu h_{11/2}, \nu g_{7/2}]$ to explain the disappearance of the signature splitting and also the enhancement of the $M1$ transition probabilities. If this were the case in ^{103}Rh, this configuration would decay preferentially to the $\pi g_{9/2}$ band as seen in the Ag isotopes. The band in ^{103}Rh is probably different from that seen in ^{105}Ag. The configuration in ^{103}Rh could be $[(\pi g_{9/2})^2, \pi p_{1/2}]_{17/2}$, which would explain the preferential decay to the $p_{1/2}$ band ($\frac{17}{2}^- \rightarrow \frac{13}{2}^-$). Perhaps these high lying levels, which seem to be part of the yrast line, arise from more complex configurations since their counterparts in ^{105}Ag seem to be more rotational. In any case, the band crossing changes the structure of the band, or, in other words, the shape of the nucleus changes, as evidenced by the enhancement of the $M1$ transition probabilities. To understand the nature of this band, one has to consider three quasiparticle configurations in the calculation with different types of coupling schemes.

Recently, high-spin states for a wide range of nuclei have been successfully studied with the cranked Nilsson-Strutinsky model.[55,56] Within this model, various high-spin features have been studied, such as shape coexistence, shape changes, band crossing, and band termination. The application of this model to ^{103}Rh may explain the high-spin features of this nucleus in more detail.

V. CONCLUSION

We have presented an extensive investigation of the nuclear structure of ^{103}Rh. More than fifteen new high-spin levels with excitation energies up to 6.2 MeV were identified for the first time.

The data for the low-lying collective negative parity band are in good agreement with calculations assuming a slightly deformed rotor. We conclude that the failure of this model in describing positive parity states with the same core parameters might be an indication of a configuration dependent deformation. The asymmetric rotor plus particle model assuming a large quadrupole deformation and $\gamma \approx 24°$ resulted in reasonable agreement with low-lying levels for both bands. The predicted electromagnetic properties of the negative parity band are in better agreement with the data than those obtained with the symmetric rotor model. However, the accuracy of the deformation parameters for the positive parity band cannot be confirmed since no $B(E2)$'s are known for this band. The IBFM-1 was the most successful model in explaining the collective structure of both bands with the same core parameters, but the agreement with the energy levels for the positive parity band was not as good as that obtained for the negative parity states. This leads to further support for shape coexistence for 1qp configurations in ^{103}Rh.

Although there are still some unresolved questions,

this study shows that due to the softness of the nucleus, the transition path may not be very well defined. But the possibility of transition from a vibrator toward γ unstable for Rh isotopes is supported by both the asymmetric rotor and the IBFM-1 calculations. The strength of different forces experienced by the nucleus changes as nucleons occupy different configurations. The difference between the two configurations $\pi p_{1/2}$ and $\pi g_{9/2}$ might be the result of the effective n-p forces which are especially strong when SOP orbitals such as $\pi g_{9/2}, \nu g_{7/2}$ and $\pi g_{9/2}, \nu h_{11/2}$ are involved.

The high-spin data showed that the alignment of a pair of $h_{11/2}$ neutrons is responsible for backbending in the mass 100 region. There is evidence for shape changes at higher excitation energies. For the unique parity band a drastic change of the energy spacings and the $M1$ transition probabilities within yrast sequence was found at spin $\frac{21}{2}^+$. This was explained as a crossing of the $g_{9/2}$ proton band with the 3qp band in which the $g_{9/2}$ proton and two aligned $h_{11/2}$ nuetrons are active. The data suggest that, in these transitional nuclei, protons in the $g_{9/2}$ orbital and neutrons in $h_{11/2}$ orbital polarize the core and imprint the geometry of their orbitals onto the nucleus. The enhancement of $M1$ transition probabilities above the crossing point can be explained partially by a shape change that occurs when the $g_{9/2}$ proton becomes more strongly coupled in the 3qp configuration and partially by the contribution of the aligned $h_{11/2}$ neutrons. These effects are expected when unique parity orbitals are involved and proton and neutron Fermi surfaces, λ_p and λ_n, lie in different parts of the j shell. Such a behavior has been observed to be more pronounced in the mass 80 region[24] than in ^{103}Rh, but less pronounced in light Ho (Ref. 22) and Tm nuclei.[23]

Clearly the $A \approx 100$ transitional nuclei, which display both collective and single-particle features, require more systematic studies of their properties. Additional work is needed to arrive at a comprehensive theoretical interpretation.

ACKNOWLEDGMENTS

We are deeply grateful to F. Rickey and P. Simms for providing us with their symmetric rotor code, the parameters used in their Ag calculations and also for helpful comments and discussion. We would especially like to thank G. Leander for generously providing us with the generalized asymmetric rotor plus particle code, the parameters for ^{103}Rh and his helpful comments. We also express our appreciation to O. Scholten for providing us with the IBM, the IBFM codes, and the ^{103}Rh parameters. We are grateful to Dr. R. M. Diamond for reading the manuscript. This work is supported in part by U. S. Department of Energy. One of us (R.P.S.) acknowledges additional support from the Robert A. Welch Foundation.

[1]E. Cheifetz, R. C. Jared, S. G. Thompson, and J. B. Wilhelmy, Phys. Rev. Lett. **25**, 38 (1970).
[2]K. Sistemich, G. Sadler, T. A. Khan, H. Lawin, W. D. Louppe, H. A. Selic, F. Schussler, J. Blachot, E. Monnand, J. P. Becquet, and B. Pfeiffer, Z. Phys. A **281**, 169 (1977).
[3]R. Bengtsson, P. Moller, J. R. Nix, and J. Zhang, Phys. Scr. **29**, 402 (1984).
[4]P. Federman and S. Pittel, Phys. Rev. C **20**, 820 (1979).
[5]P. Federman, S. Pittel, and R. Campos, Phys. Lett. **82B**, 9 (1979).
[6]J. A. Grau, L. E. Samuelson, F. A. Rickey, P. C. Simms, and G. J. Smith, Phys. Rev. C **14**, 2297 (1976).
[7]J. Rekstad, Nucl. Phys. **A247**, 7 (1975).
[8]H. A. Smith and F. A. Rickey, Phys. Rev. C **14**, 1946 (1976).
[9]Rakesh Popli, J. A. Grau, S. I. Popik, L. E. Samuelson, F. A. Rickey, and P. C. Simms, Phys. Rev. C **20**, 1350 (1979).
[10]Ch. Vieu, S. E. Larsson, G. Leander, I. Regnarsson, and J. S. Dionision, Phys. Rev. C **22**, 853 (1980).
[11]P. Van Isacker and G. Puddu, Nucl. Phys. **A348**, 125 (1980).
[12]A. Arima and F. Iachello, Ann. Phys. (NY) **99**, 253 (1976).
[13]N. Kaffrell, N. Trautmann, and G. Herrmann, Phys. Rev. C **8**, 320 (1973); J. Stachel *et al.*, Nucl. Phys. **A383**, 429 (1982); J. Stachel *et al.*, *ibid.* **A419**, 589 (1984).
[14]M. F. Nolan, J. Hall, D. J. Thomas, and M. J. Throop, J. Phys. A **6**, L587 (1973).
[15]A. Bockisch, M. Miller, A. M. Kleinfeld, A. Gelberg, and U. Kaup, Z. Phys. A **292**, 265 (1979).
[16]A. Gelberg, B. Herskind, R. Kalish, and M. Neiman, Z. Phys. A **279**, 183 (1976).
[17]A. Christy, I. Hall, R. P. Harper, I. M. Naqib, and B. Wakefield, Nucl. Phys. **A142**, 591 (1970).
[18]A. Arseniev, A. Sobiczewski, and V. G. Soloview, Nucl. Phys. **A139**, 269 (1969).
[19]A. Faessler, J. E. Galonska, V. Gotz, and H. C. Pauli, Nucl. Phys. **A230**, 302 (1974).
[20]F. K. McGowan, R. L. Robinson, P. Stelson, and T. Miller, Nucl. Phys. **A113**, 529 (1968).
[21]M. J. A. de Voigt, J. Dubek, and Z. Szymanski, Rev. Mod. Phys. **55**, 949 (1983),
[22]G. B. Hagemann, J. D. Garrett, B. Herskind, G. Sletten, P. O. Tjom, A. Henriques, F. Ingebretsen, J. Rekstad, G. Lovhoiden, and T. F. Thorsteinsen, Phys. Rev. C **25**, 3224 (1982).
[23]A. J. Larabee, L. H. Courtney, S. Frauendorf, L. L. Riedinger, J. C. Waddington, M. P. Fewell, N. R. Johnson, I. Y. Lee, and K. K. McGowan, Phys. Rev. C **29**, 1934 (1984).
[24]L. Funke, F. Donau, J. Doring, P. Kemnitz, E. Will, G. Winter, L. Hildingsson, A. Johnson, and Th. Lindblad, Phys. Lett. **120B**, 301 (1983).
[25]S. Frauendorf, *Proceeding of International Symposium In-Beam Nuclear Spectroscopy* (Debrecen, Hungary, 1984).
[26]D. R. Haenni, H. Dejbakhsh, R. P. Schmitt, and G. Mouchaty, Phys. Rev. C **33**, 1543 (1986).
[27]*Table of Isotopes*, 7th ed., edited by C. M. Lederer and V. S. Shirely (Wiley, New York, 1978), p. 453.
[28]R. O. Sayer, J. Temperley, and D. Eccleshall, Nucl. Phys. **A179**, 122 (1972).
[29]J. A. Barclay, S. S. Rosenblum, W. A. Steyert, and K. S. Krane, Phys. Rev. C **14**, 1183 (1976).
[30]G. Kajrys, S. Landsberger, and S. Monaro, Phys. Rev. C **28**,

2335 (1983).
[31]A. Charvet, R. Duffait, R. Beraud, K. Duffait, A. Emsallem, M. Meyer, J. Treherne, and A. Gizon, Z. Phys. A **315**, 163 (1984).
[32]H. Dejbakhsh, D. R. Haenni, R. P. Schmitt, and G. Mouchaty, Bull. Am. Phys. Soc. **28**, 976 (1983); **30**, 1258 (1985).
[33]D. R. Haenni, H. Dejbakhsh, R. P. Schmitt, and G. Mouchaty, American Chemical Society Symposium Series No. **324**, 1985, edited by R. A. Meyer and D. S. Brenner (ACS), Washington, D.C., 1986), p. 331.
[34]W. B. Ewbank, Nucl. Data Sheets **28**, 403 (1979).
[35]J. T. Routti and S. G. Prussin, Nucl. Instrum. Methods **72**, 125 (1969).
[36]M. E. Bunker and C. W. Reich, Rev. Mod. Phys. **43**, 348 (1971).
[37]F. S. Stephens, R. M. Diamond, and S. G. Nilsson, Phys. Lett. **44B**, 429 (1973); F. S. Stephens, Rev. Mod. Phys. **47**, 43 (1975).
[38]B. Reehal and R. Sorensen, Phys. Rev. C **2**, 819 (1970).
[39]L. E. Larsson, G. Leander, I. Ragnarson, and N. G. Alenius, Nucl. Phys. **A261**, 77 (1976).
[40]A. Bohr and B. Mottelson, *Nuclear Structure* (Benjamin, New York, 1969), Vol. I, p. 169.
[41]M. Mariscotti, G. Goldhaber, and B. Buck, Phys. Rev. **178**, 1864 (1969).
[42]V. Paar, Nucl. Phys. **A211**, 29 (1973).
[43]K. Heyde and V. Paar, Phys. Lett. B **179**, 1 (1986).
[44]P. C. Simms, F. A. Rickey, and R. K. Popli, Nucl. Phys. **A347**, 205 (1980).
[45]R. F. Casten, in *Interacting Boson-Fermi System in Nuclei*, edited by F. Iachello (Plenum, North-Holland, 1981), p. 317.
[46]D. Ballon, Y. Niv, S. Vajda, N. Benczer-Koller, L. Zamick, and G. Leander, Phys. Rev. C **33**, 1461 (1986).
[47]S. E. Larsson, G. Leander, and I. Ragnarsson, Nucl. Phys. **A307**, 189 (1978).
[48]F. Iachello, *Interacting Boson in Nuclear Physics* (Plenum, New York, 1979), p. 1.
[49]J. Jolie, P. Van Isacker, K. Heyde, J. Moreau, G. Van Landeghem, M. Waroquier, and O. Scholten, Nucl. Phys. **A438**, 15 (1985).
[50]P. De Gelder, D. De Frenne, K. Heyde, and N. Kaffrell, Nucl. Phys. **A401**, 397 (1983).
[51]R. F. Casten, Phys. Rev. Lett. **54**, 1991 (1985).
[52]H. Dejbakhsh and R. P. Schmitt (unpublished).
[53]F. Donau, *Proceedings of International Symposium on In-Beam Nuclear Spectroscopy* (Debrecen, Hungary, 1984), p. 701.
[54]H. J. Keller, S. Frauendorf, U. Hagemann, L. Kaubler, H. Prade, and F. Stary, Nucl. Phys. **A444**, 261 (1985).
[55]T. Bengtsson and I. Ragnarsson, Nucl. Phys. **A436**, 14 (1985).
[56]W. Nazarewicz, J. Dudek, R. Bengtsson, T. Bengtsson, and I. Regnarsson, Nucl. Phys. **A435**, 397 (1985).